AGU PUBLICATIONS

JGR

Journal of Geophysical Research: Oceans

RESEARCH ARTICLE

10.1002/2016JC011764

**Key Points:**
- Plume is composed of narrow region of rising water and wider surface expression
- Plume models reproduce the basic dynamical characteristics of the plume
- Plume surface waters are ~10% subglacial discharge and ~90% entrained fjord waters

**Correspondence to:**
K. D. Mankoff,
mankoff@psu.edu

**Citation:**
Mankoff, K. D., F. Straneo, C. Cenedese, S. B. Das, C. G. Richards, and H. Singh (2016), Structure and dynamics of a subglacial discharge plume in a Greenlandic fjord, *J. Geophys. Res. Oceans*, *121*, 8670–8688, doi:10.1002/2016JC011764.

Received 29 FEB 2016
Accepted 15 OCT 2016
Accepted article online 19 OCT 2016
Published online 15 DEC 2016



# Structure and dynamics of a subglacial discharge plume in a Greenlandic fjord

**Kenneth D. Mankoff[1,2], Fiammetta Straneo[1], Claudia Cenedese[1], Sarah B. Das[3], Clark G. Richards[1,4], and Hanumant Singh[5,6]**

[1]Department of Physical Oceanography, Woods Hole Oceanographic Institution, Woods Hole, Massachusetts, USA, [2]Department of Geosciences, Pennsylvania State University, University Park, Pennsylvania, USA, [3]Department of Geology and Geophysics, Woods Hole Oceanographic Institution, Woods Hole, Massachusetts, USA, [4]RBR Ltd., Ottawa, Ontario, Canada, [5]Department of Applied Ocean Physics and Engineering, Woods Hole Oceanographic Institution, Woods Hole, Massachusetts, USA, [6]Department of Electrical and Computer Engineering, Northeastern University, Boston, Massachusetts, USA

**Abstract** Discharge of surface-derived meltwater at the submerged base of Greenland's marine-terminating glaciers creates subglacial discharge plumes that rise along the glacier/ocean interface. These plumes impact submarine melting, calving, and fjord circulation. Observations of plume properties and dynamics are challenging due to their proximity to the calving edge of glaciers. Therefore, to date information on these plumes has been largely derived from models. Here we present temperature, salinity, and velocity data collected in a plume that surfaced at the edge of Saqqarliup Sermia, a midsized Greenlandic glacier. The plume is associated with a narrow core of rising waters approximately 20 m in diameter at the ice edge that spreads to a 200 m by 300 m plume pool as it reaches the surface, before descending to its equilibrium depth. Volume flux estimates indicate that the plume is primarily driven by subglacial discharge and that this has been diluted in a ratio of 1:10 by the time the plume reaches the surface. While highly uncertain, meltwater fluxes are likely 2 orders of magnitude smaller than the subglacial discharge flux. The overall plume characteristics agree with those predicted by theoretical plume models for a convection-driven plume with limited influence from submarine melting.

## 1. Introduction

Calving of icebergs and submarine melt account for approximately 50% of the mean annual freshwater discharge from the Greenland Ice Sheet with runoff accounting for the remainder [*Bamber et al.*, 2012; *Enderlin et al.*, 2014]. The relative importance of calving versus submarine melt, however, varies considerably depending on the particular glacier [*Enderlin and Howat*, 2013]. Neither calving nor submarine melting is well understood but both are thought to be enhanced in the presence of subglacial discharge plumes generated by the large volumes of supraglacial meltwater that flows through and from the ice sheet each melt season [*Chu*, 2013]. Specifically, enhanced turbulence driven by the release of buoyant water at depth is thought to increase submarine melt by increasing mixing across the ice/ocean boundary layer [*Jenkins*, 2011; *Xu et al.*, 2013; *Sciascia et al.*, 2013; *Kimura et al.*, 2014; *Slater et al.*, 2015; *Motyka et al.*, 2013]. Beyond the direct mass loss, undercutting due to localized melt associated with subglacial discharge plumes also changes the stress state of the glacier terminus and may enhance calving [*O'Leary and Christoffersen*, 2013].

Our understanding of the dynamics of these plumes is limited. It is generally accepted that this buoyant freshwater injection generates regions of rising fluid that progressively entrain saltier, denser seawater and that the associated submarine melting of the ice front adds a third water type to the rising mixture [*Jenkins*, 2011]. If this mixture reaches the surface, it is typically visible as a localized patch of sediment-laden waters that spreads away from the glacier terminus [*Chauché et al.*, 2014]. Not all plumes reach the surface, however, in which case they are not detectable at the surface [e.g., *Chauché et al.*, 2014; *Stevens et al.*, 2016].

In situ observations of plumes are scarce due to their proximity to the dangerous calving glacier margin. Temperature and salinity profiles have been collected in plumes at the margins of Greenlandic glaciers, one each described in *Hartley and Dunbar* [1938], *Chauché et al.* [2014] and *Bendtsen et al.* [2015]. In all cases,

the temperature and salinity properties and high turbidity values are indicative of high concentrations of subglacial discharge, upwelling of fjord waters from depth and limited submarine melting. No velocity measurements within a plume have been made, to our knowledge. What are more common, instead, are observations of glacially modified waters containing both submarine melt and subglacial discharge at distances greater than 500 m from the glacier front [e.g., *Straneo et al*., 2011, 2012; *Mortensen et al*., 2013; *Kjeldsen et al*., 2014; *Beaird et al*., 2015]. Because of where they are collected, however, the modification of these waters cannot be attributed to plume processes alone, rather they represent the integrated effects of plume and fjord scale processes. Thus, from these observations alone, one cannot infer the dynamics and structure of the plumes at the glacier front [*Stevens et al*., 2016].

Theoretical and numerical studies of plumes at the ice edge have been instrumental in partially addressing this knowledge gap. Numerical simulations of plumes driven by localized subglacial discharge show that, in the near-ice environment ($<$50–100 m from the ice face), modeled plumes compare relatively well with classical plume theory [*Salcedo-Castro et al*., 2011; *Xu et al*., 2012, 2013; *Sciascia et al*., 2013; *Kimura et al*., 2014; *Carroll et al*., 2015; *Slater et al*., 2015]. Further away from the glacier, however, the large scale circulation and distribution of properties associated with the plumes depends on processes not accounted for in plume theory [*Sciascia et al*., 2013; *Carroll et al*., 2015]. The impact of plumes on melt rates has been explored in these models using melt rate parameterizations (typically *Holland and Jenkins* [1999]). Both idealized plume models and more complex numerical simulations show that melt rates in the "plume region" increase with increasing subglacial discharge and largely attribute this increase to the localized velocity increase associated with rising plumes [*Jenkins*, 2011; *Sciascia et al*., 2013; *Xu et al*., 2013; *Kimura et al*., 2014]. The release of submarine melt (i.e., fresh water directly from the ice front) within a plume, furthermore, can impact the plume dynamics and feedback on the melt rate.

The extent to which either the idealized plume models or the more sophisticated numerical models actually capture the leading order dynamics at the ice edge, however, is largely unknown because of the lack of observations required to validate these models. Furthermore, the wide range of spatial scales involved (from centimeters at the ice edge to tens of kilometers at the fjord scale) poses a major computational challenge. As a result, turbulent processes cannot be fully resolved and need to be parameterized, making the results sensitive to the viscosity and diffusivity parameters within the model. The turbulent entrainment is fundamental for the dynamics of a plume and is often parameterized as either a diffusive process [*Xu et al*., 2012; *Sciascia et al*., 2013] or the plume itself is represented via a theoretical model [e.g., *Cowton et al*., 2015].

In this study, we use data collected in July 2013 at the margin of Saqqarliup Sermia, a midsize glacier in West Greenland where a persistent patch of sediment-rich water spreading from the glacier front indicated the existence of one major plume fed by subglacial discharge. A survey conducted the previous year (July 2012) at the margin of this same glacier, extending from the far-field to within $\sim$100 m of the glacier face, identified this as one of two major subglacial discharge locations by mapping the distribution of glacially modified waters [*Stevens et al*., 2016]. That study showed that, at a distance of $\sim$150 m from the glacier face, the mixture of subglacial discharge, submarine melt, and ambient water entrained in the plume had already equilibrated at its neutral buoyancy depth and was spreading horizontally. The implication is that the region of upwelling at the ice edge was narrower than $\sim$150 m.

Here we present data collected closer to the ice front, in a survey within 100 m of the glacier. In particular, we identify a turbulent patch that is the surface expression of a plume driven by localized subglacial discharge. We use a combination of water temperature, salinity, and velocity data obtained within this patch to estimate, for the first time, volume fluxes. Furthermore, by combining the patch volume flux estimates with estimates of subglacial discharge volume flux, we test the validity of classical plume theory.

## 2. Field Site and Data

The field campaign took place in central West Greenland in the Saqqarliup Sermia/Saqqarliup Fjord outlet system, the southern-most branch of Ilulissat Icefjord [*Bjørk et al*., 2015]. The fjord is on average 150 m deep, 6 km wide at the glacier front, 2.5 km wide 5 km from the glacier front and 35 km long. A $\sim$70 m deep sill was mapped $\sim$16 km from the ice front [*Stevens et al*., 2016] (Figure 1). Saqqarliup Sermia is a 6 km wide outlet glacier of the Greenland Ice Sheet characterized by speeds of 150 m yr$^{-1}$ [*Joughin et al*., 2013].

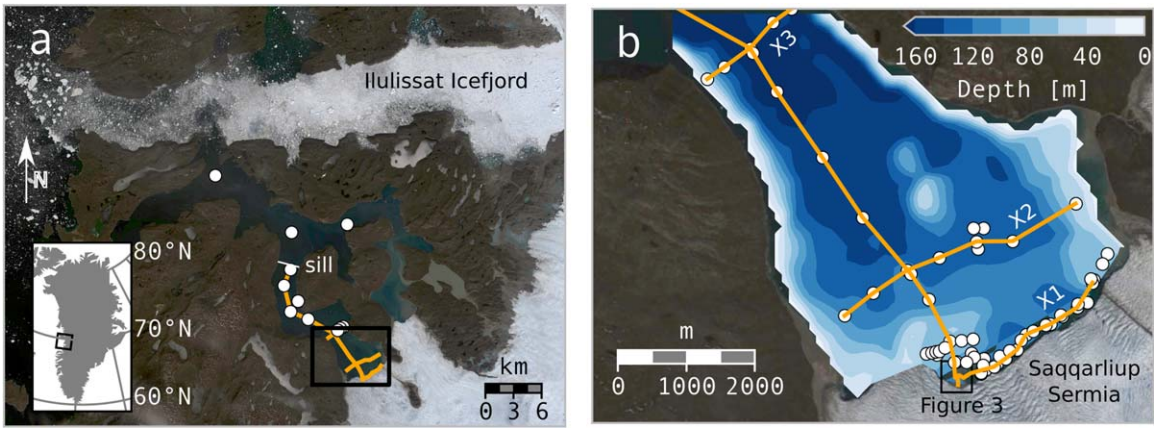


**Figure 1.** Overview of Saqqarliup Fjord in central West Greenland, the southern-most branch of Ilulissat Icefjord. Black box in inset marks location of Figure 1a. Black box in Figure 1a marks location of Figure 1b. Black box in Figure 1b marks location of Figure 3. White dots are (X)CTD cast locations. Orange lines mark (X)CTD transects shown in Figures 7 and 8. The subglacial discharge is at ~150 m depth and located at the ice edge just south of the along-fjord transect line. Bathymetry is from *Stevens et al.* [2016]. Background Landsat scene is a panchromatic enhanced view of #LC80100112013172LGN00 from 21 June 2013, ~1 month prior to the fieldwork.

This relatively slow velocity, approximately 1% of the nearby fast-flowing Jakobshavn Isbræ glacier, and associated weak calving, allowed us to map the plume behavior over several days. The average fjord depth along the grounded glacier front is ~150 m. The terminus position has been relatively stable over the satellite record with a ~1 km retreat since 1992 [*Stevens et al.*, 2016]. This glacier/fjord system has a catchment area of 400 ± 50 $km^2$ and an estimated annual runoff of 1 $km^3$ $yr^{-1}$ which is divided into three subcatchment basins [*Stevens et al.*, 2016].

We collected data from 24 to 31 July 2013 using a small boat, a remote-controlled surface vehicle called the JetYak (Figure 2) [*Kimball et al.*, 2014], and a helicopter. Aerial and satellite photographs complement the in situ measurements. A persistent patch of sediment-laden waters characterized by high horizontal velocity was observed during the entire field campaign (Figure 3). We interpret this patch as the surface expression of an upwelling plume fed by the localized subglacial discharge at depth of surface-derived meltwater runoff. Its location coincided with that of a core of subsurface, glacially modified waters observed in July 2012 and attributed to the discharge at depth of surface runoff from the main Saqqarliup Sermia subcatchment basin [*Stevens et al.*, 2016]. During the 2012 field campaign, however, no surface expression of a plume was observed. Throughout this study, we reserve the term "plume" for the near-ice feature characterized by a *plume core* and a *plume pool*. The plume core is the vertically rising and typically ice-attached volume of water forced by localized subglacial discharge. The plume pool is the near-surface and surface signature above the core.

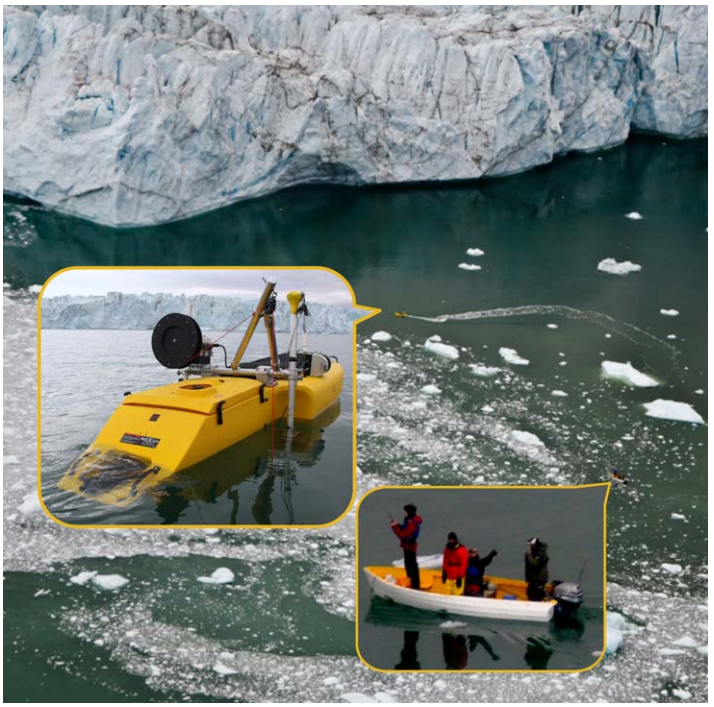

**Figure 2.** Photograph of the JetYak as it approaches the glacier face taken from a helicopter. Inserts show a picture of the JetYak and of the boat from which it was controlled.

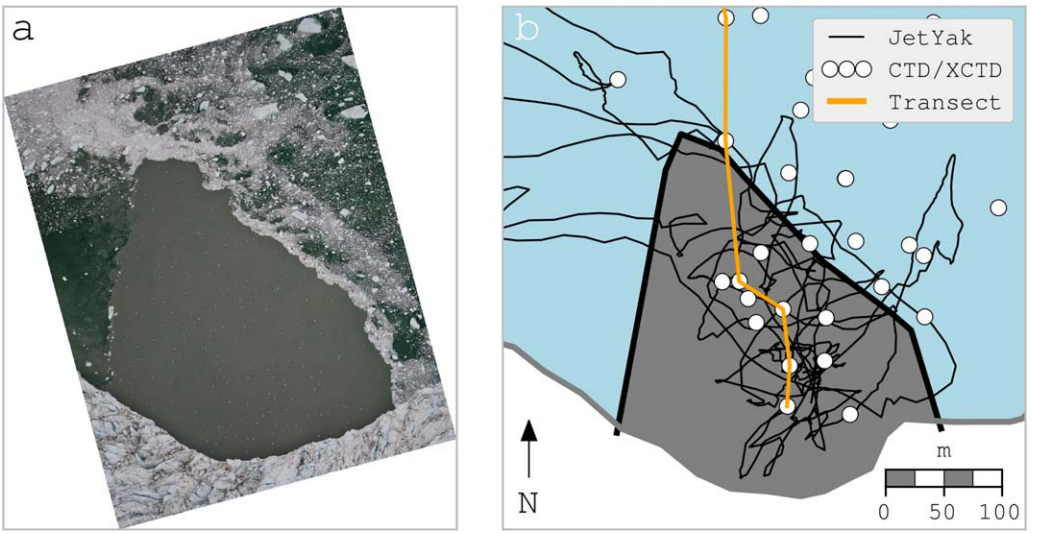


**Figure 3.** (a) Photograph of plume pool from helicopter and (b) locations of (X)CTDs (white circles). Orange line (same as in Figure 1) shows the location of the along-fjord transect (Figure 7). Background colors are glacier (white), fjord (blue) and pool (gray), with boundaries digitized from Landsat scene acquired ~1 month prior to photograph and shown in Figure 1. Thin black line is JetYak path (also shown in Figure 4).

During the 8 day survey period, we collected 89 CTD (conductivity, temperature, and depth) profiles using an RBR XR620 from the boat and deployed 9 Sippican XCTDs (expendable CTDs) from the helicopter. Of these, eight CTDs and four XCTDs were through the pool waters, and ~60 more were within 100 m of the pool and ice front (Figure 4). None were in the plume core below the pool. Profiles are averaged into 1 m depth bins unless otherwise specified.

The JetYak towed an RBR*concerto* CTD and an acoustic Doppler current profiler (ADCP, RDI 300 kHz) on a side-mounted pole. Position, orientation, and vehicle velocity information comes from an onboard GPS, compass, and inertial measurement unit [*Kimball et al.*, 2014]. The CTD towed by the JetYak was generally mounted to sample the surface layer just next to the JetYak. In a few instances, we attempted to collect a profile by lowering the CTD using a winched system. However, the large relative velocity between the JetYak and the water caused the CTD to trail behind the JetYak effectively continuing to collect data in the upper 10 m only. Here we use data collected over ~2 h of CTD towing on 27 July 2013 and limited to the top 10 m of the water column and in the plume pool. These CTD data are presented averaged into 1 min bins, with the mean distance covered per bin at ~25 m (assuming JetYak speeds of $<0.5$ m s$^{-1}$). Calibration of both CTDs occurred before and after use. We detected no offset between instruments and no drift over time and make no adjustments to the recorded data other than converting values to conservative temperature ($\Theta$) and absolute salinity ($S_A$) (IOC, SCOR, and IAPSO 2010), using the python port (gsw v. 3.0.3) of the thermodynamic equation of state, TEOS-10 [*McDougall and Barker*, 2011].

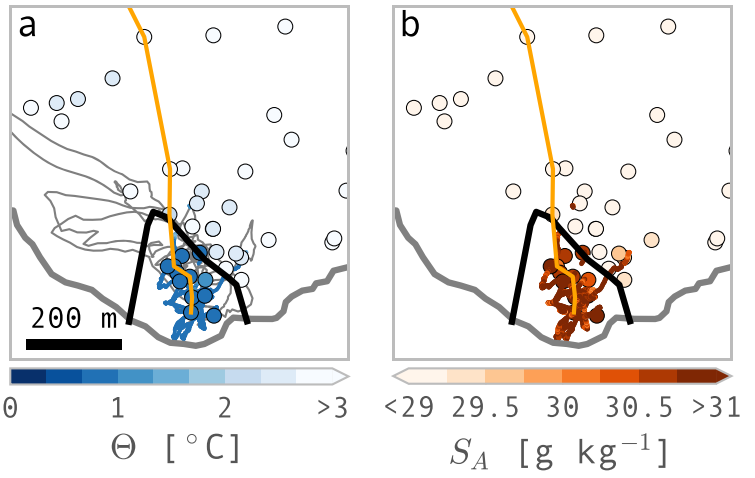


**Figure 4.** (a) Plume surface temperature and (b) surface salinity. Temperature and salinity surface properties are the average of the top 10 m of the water column. Circles are (X)CTDs from boat and helicopter. The JetYak trail is shown as a thin gray line or colored as temperature or salinity when the surface-towed CTD was deployed. Thick gray line represents the ice front from the Landsat scene in Figure 1.

We piloted the JetYak across the plume on 26 July 2013. The ADCP recorded horizontal velocity in 16 depth bins, at 4 m intervals, from 7 to 71 m below the surface. These data were recorded at ~1 Hz over 16 min with an estimated single ping uncertainty of 3.55 cm $s^{-1}$. We show velocity profiles both as a function of depth and in plan view. To obtain a mean profile of horizontal velocity within the plume, we averaged profiles collected within 100 m of the center of the plume/ice edge (more detail in section 3.2.2). Maps of the horizontal velocity at different depths are obtained by spatially binning the ADCP in a given depth bin into 10 m × 10 m spatial bins. During the plume survey, the JetYak moved slowly or held station relative to the ice and land. The 10 $m^2$ bin size, and the large relative velocity between the JetYak and waters in the pool, allowed for at least a partial averaging over the large variability observed in the plume pool associated with transiting eddies, which were also visible from the small boat. The ADCP currents were not detided, though the period of sampling in the plume occurred at high tide (i.e., slack water). Observations of currents in the top 10 m from a moored current meter located approximately 2 km ocean-ward from the plume indicate that the tidal velocities are less than 0.14 m $s^{-1}$ 95% of the time, supporting the assumption that the plume velocities are much larger than the background/tidal currents.

During our survey, we found no statistical difference between CTD/XCTD casts taken on different days, and the sediment-patch (Figure 3) maintained a qualitatively similar visual signature.

## 3. Results

### 3.1. Pool and Fjord Observations

We observe a triangular patch of anomalous water properties at the fjord surface which we identify as the plume pool (pool, hereafter), i.e., the surface expression of a buoyant plume fed by subglacial discharge. The pool has a base against the ice edge approximately 200 m wide and extends 300 m downfjord from the ice front (Figures 3 and 4). It is characterized by anomalously cold temperature, relatively high salinity, and high horizontal velocity relative to the surrounding waters. Outside the pool, the fjord is a mostly homogeneous 1°C, except for the warm surface layer. A slightly colder ~0.8°C layer is found between 25 and 40 m depth (Figure 5).

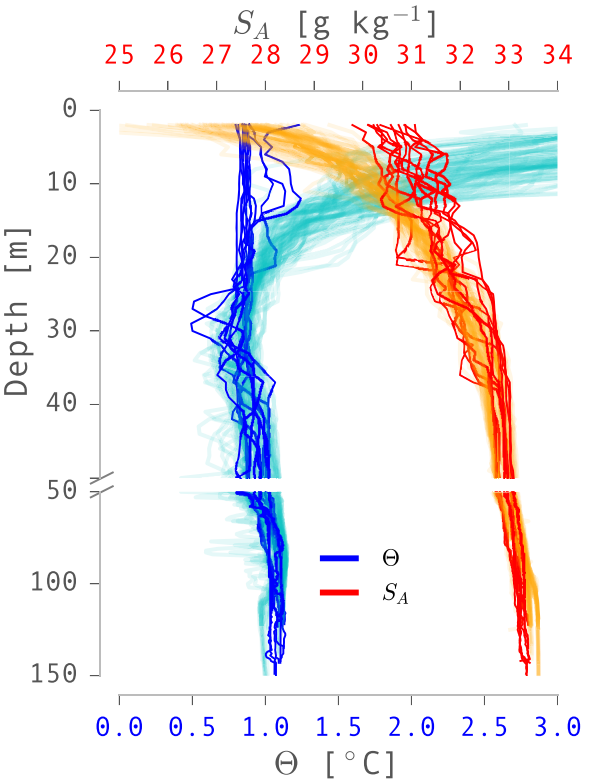


**Figure 5.** Temperature and salinity plotted against depth. Thin lines show all temperature (Θ, left, cyan, bottom axis) and salinity ($S_A$, right, orange, top axis) profiles that did not sample the pool, and the thick blue and red lines are (X)CTD casts dropped through the plume pool. The scale on the *y* axis and in other figures changes below 50 m because there is little variability below this depth and the focus is on the near-surface waters.

The lateral extent of the pool at the surface can be defined using the large temperature or salinity anomalies that characterize the pool waters and is not overly sensitive to the property or the value used. We define it as that region whose average Θ over the top 10 m is <1.33°C. Anomalies decrease rapidly with depth making it challenging to define the bottom boundary of the pool in Θ or $S_A$. Instead, we define the bottom of the pool by using the horizontal velocity data collected by the JetYak. Using data collected within a 100 m radius of the midpoint of the pool at the glacier/ocean front (Figure 6, dashed semicircular region in subplots), we find that the core of the velocity within the pool is aligned along a bearing of 338°, roughly parallel to the downfjord direction and orthogonal to the glacier terminus (Figure 6). Thus, we define a plume-aligned coordinate

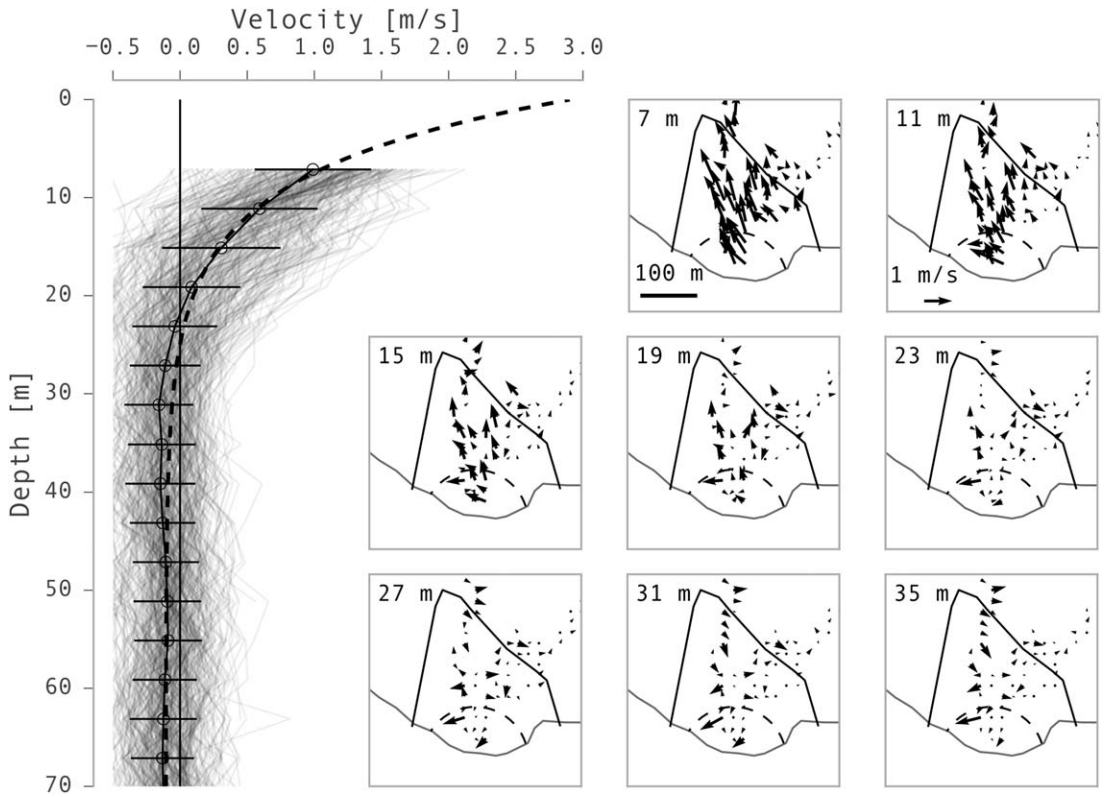


**Figure 6.** Along-plume velocity versus depth in the plume pool from JetYak ADCP. (left) Individual velocity-depth profiles (gray lines), standard deviation from mean value (circles and horizontal bars), and an exponential fit (dashed line). Profiles are limited to data collected within 100 m of the ice front and inside the pool boundary (inside dashed semicircle in subplots). Vertical line at 0 separates positive values away from the ice and negative values toward the ice. Small plan view subplots show all velocities in the depth bin labeled in each plot, binned 10 m horizontally. Thin gray line is ice front, black line is plume pool surface boundary (approximate) shown in Figure 3, and dashed semicircle marks 100 m from plume/ice center and the subset used in main plot.

system by rotating velocities in an along-plume and across-plume direction—which we will use for the remainder of the paper.

The average along-plume velocity profile decreases with depth but is still generally away from the ice in the top 20 m. At approximately 20 m depth, the average along-plume velocity is zero and we define this as the maximum pool depth, $d_p$ (Figure 6). We estimate the maximum along-plume velocity in the pool to be $\sim$3 m s$^{-1}$ at the surface by extrapolation using an exponential fit to the mean along-plume velocity profile (residual standard error is 4 cm s$^{-1}$). We obtain a similar value by computing the average drift speed of the JetYak after we put it in neutral and let it drift within the plume. The average along-plume velocity over the upper 20 m derived from the extrapolated profile is 0.84 m s$^{-1}$. We note that around a depth of 30 m, it appears that the flow direction is reversed (i.e., the mean flow is toward the ice) but the signal is small relative to the variability (Figure 6).

A CTD transect from the ice edge to the fjord sill (orange line along fjord in Figure 1) shows that the plume region is characterized by anomalously dense, cold waters at the surface with $\sigma = 25$ kg m$^{-3}$ and anomalously cold waters with $\sigma = 26$ kg m$^{-3}$ at a depth of 35 m (Figure 7, top). Stratification is primarily controlled by salinity (Figure 7, bottom). This anomalous cold, subsurface layer is present throughout the fjord as seen in the along-fjord transect and in a series of cross-fjord transects parallel to the glacier face (Figure 8). This layer becomes progressively warmer in transects farther away from the glacier face (Figure 8) indicating that it is produced at the glacier/ocean interface.

A $\Theta - S_A$ plot (Figure 9) clarifies the origin of the different water masses present in the fjord, in the pool and in the vicinity of the plume. In it, we include all of the casts shown in Figure 5, plus all the CTD samples from the plume pool collected by the CTD on JetYak (black dots in Figure 9), which only sampled the upper 10 m. Profiles that sampled the pool (bold lines in Figure 5) are separated into an upper layer within the pool (orange dots in Figure 9, $<$20 m depth) and data below the pool (blue dots in Figure 9, $>$20 m depth).

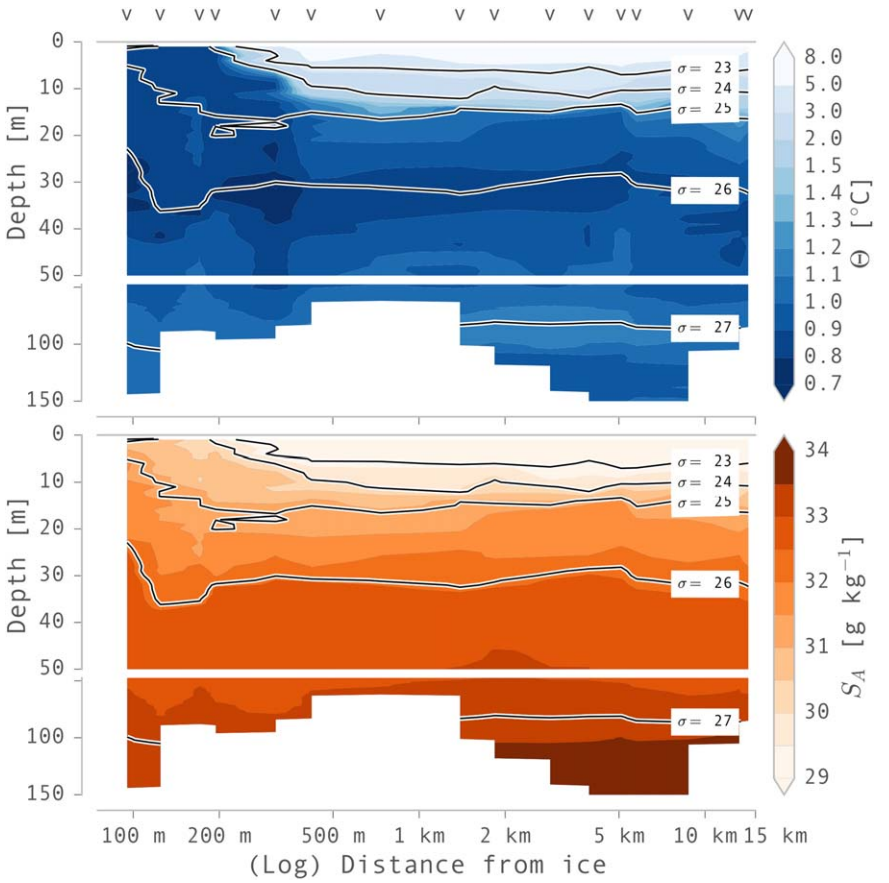


**Figure 7.** (top) Temperature and (bottom) salinity transects from the ice (left edge of figure) to the end of the along-fjord orange line in Figure 1. Axes are nonlinear with logarithmic *x* axis and change in *y* axis scale below 50 m depth as in Figure 5. "v" symbols mark cast locations.

Profiles collected close to the fjord's mouth both inside and outside the sill provide far-field context to the data shown. As discussed in *Stevens et al.* [2016], the deep waters flowing into the fjord are those found roughly at sill depth outside the fjord, relatively warm and salty waters flowing in from Ilulissat Icefjord. For waters less dense than $\sigma = 26.25$ kg m$^{-3}$, water properties in the vicinity of the glacier are different from those observed near the mouth—suggesting these waters are glacially modified waters resulting from glacier/ocean interaction [e.g., *Straneo et al.*, 2011]. Specifically, these waters are largely contained within subglacial discharge and meltwater mixing lines (see section 3.2.1) that start from the point in $\Theta - S_A$ space that corresponds to the properties of waters near the glacier at the grounding line depth (see section 3.2.1) [*Jenkins*, 2011]. Thus, the properties of these waters can be explained by the combined effect of submarine melting at the glacier face and the discharge of freshwater (subglacial discharge) at the base of the glacier. Within these new water masses is the cold ($\Theta < 0.8$°C) water mass at $\sigma = 26$ kg m$^{-3}$ observed under the pool and throughout the fjord, whose temperatures can be as low as 0.5°C. This cool layer is indicative of submarine melting either in the plume region or along the glacier face. It is impossible, without additional data, to establish the exact origin of these waters. However, the fact that this layer is present along the entire glacier face (Figure 8, X1) and that just beyond the plume region this layer is seen flowing *toward* the plume (Figure 6) suggests that these waters may be produced by submarine melt both in the plume region but also along the entire glacier face. Compared to this cold subsurface layer, the waters observed in the pool are considerably fresher. As shown in section 3.2.1, these properties are indicative of rapid, turbulent mixing of subglacial discharge waters released at depth with the deep, ambient waters of the fjord.

The properties and velocity distribution observed within the pool confirm that it is the surface expression of an upwelling plume driven primarily by the release of subglacial discharge at depth (Figure 10). This interpretation is consistent with observations conducted during a survey the previous year when a core of

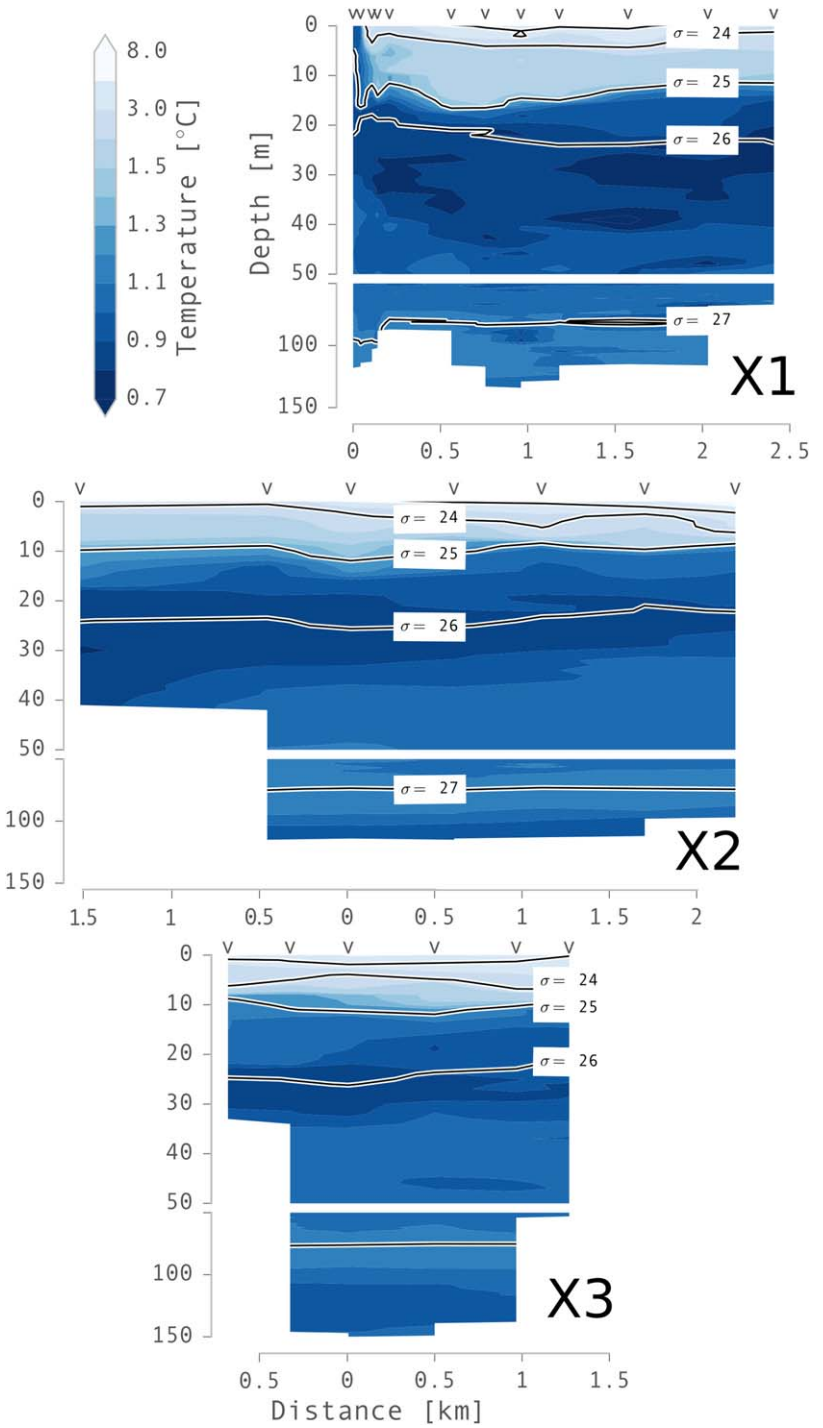


**Figure 8.** Cross-fjord temperature transects. X1, X2, and X3 are located at orange lines X1, X2, and X3 in Figure 1b. Horizontal axis is aligned with 0 at the along-fjord transect. Observer is at the glacier south of the transects looking north toward the fjord mouth. *y* axes are nonlinear with change in scale below 50 m depth as in Figure 5. "v" symbols mark cast locations.

subsurface, glacially modified waters was observed within 300–500 m of the ice edge at the same location [*Stevens et al.*, 2016]. Several of the plume features are also qualitatively consistent with numerical simulations of subglacial discharge plumes, e.g., the overshoot [*Sciascia et al.*, 2013] and the lateral spreading of the plume once it reaches the surface [*Kimura et al.*, 2014].

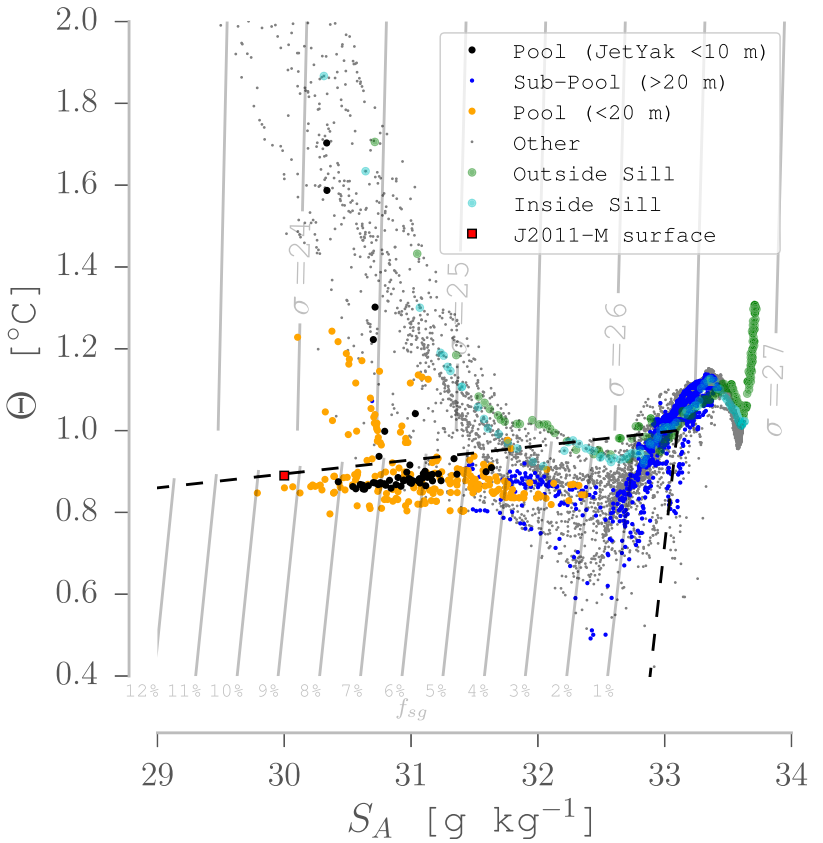


**Figure 9.** Salinity versus temperature ($\Theta$–$S_A$) plot. Black dots are from the JetYak surface-towed CTD. Orange dots are from non-JetYak (X)CTD samples in the pool (bold lines at depths of <20 m in Figure 5), and blue from those same casts but below the pool (bold lines at depth >20 m in Figure 5). Small gray dots are all other casts in the fjord (thin lines in Figure 5). Cyan and green are from casts just inside and outside the sill (Figure 1), respectively. Red square is model results at model surface. Inner grid shows the fraction of subglacial discharge ($f_{sg}$). Near-vertical lines above show $\sigma$ density contours. Dashed lines represent freshwater subglacial discharge mixing line (near horizontal) and submarine meltwater mixing line (near vertical).

### 3.2. Water Mass Analysis

#### 3.2.1. Theory

To obtain greater insight into the dynamics at the ice edge, we make the assumption that the water properties can be described as a mixture of three different water masses: (1) subglacial discharge (surface-derived glacier meltwater discharged at the grounding line), (2) submarine meltwater (meltwater generated locally through the melting of the glacier face), and (3) entrained water (the ambient waters that are entrained by the rising plume). A further assumption is that diffusion of temperature and salinity is negligible. These assumptions have previously been used in glacier/fjord studies in Greenland to estimate the volume fraction of different water masses present in the fjord [e.g., *Mortensen et al.*, 2013]. As shown by *Beaird et al.* [2015], this approach leads to an underconstrained system in many Greenlandic fjords because the number of water masses generally exceeds the available variables. In the case studied here, however, use of this model can be justified if one assumes that the bulk of the entrainment within the rising plume occurs below 20–30 m, where the ambient fjord waters are largely homogeneous (Figure 5). In this case, the fjord waters can be reasonably well characterized by a single water mass and the number of variables (salt, temperature, and mass) and the number of waters masses is the same.

The three-mass mixing model is based on volumetric water mass fractions and described by the following equations, beginning with volume conservation,

$$f_{sg}+f_{mw}+f_e=1, \tag{1}$$

where $f_{sg}$, $f_{mw}$, and $f_e$ are the volume fractions of subglacial discharge, submarine meltwater, and entrained water, respectively. Salt conservation implies

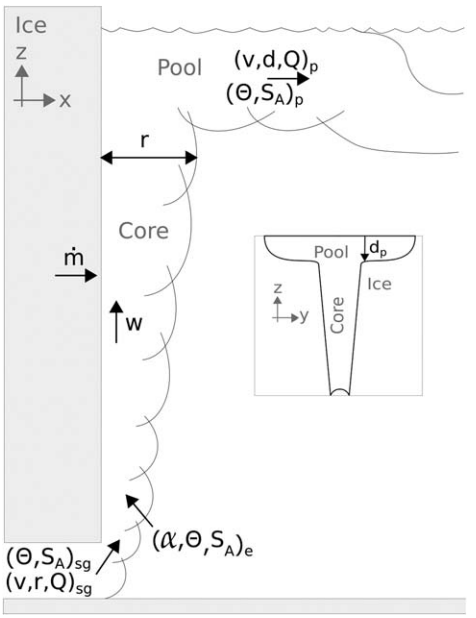


**Figure 10.** Schematic of a subglacial discharge plume in a fjord. This schematic shows subglacial properties (*sg*) entering a fjord, entraining (*e*) fjord waters, and rising up the ice front as a plume core small relative to the surface expression, then expanding near the surface, where pool (*p*) properties are a combination of the subglacial (*sg*) and entrained (*e*) properties.

$$S_A = f_e S_{Ae}, \tag{2}$$

where $S_A$ is the sampled salinity, and $S_{A_e}$ is the entrained salinity. Heat conservation implies

$$\Theta = \Theta_{sg} f_{sg} + \Theta_{mw} f_{mw} + \Theta_e f_e, \tag{3}$$

with $\Theta$ the sampled conservative temperature, $\Theta_{sg}$ the conservative temperature of the subglacial discharge, $\Theta_{mw}$ the conservative temperature of submarine meltwater, and $\Theta_e$ the conservative temperature of the entrained water.

Unique to the melting of ice, the "properties" of the submarine meltwater take into account the cooling resulting from the heat extracted to melt the ice [*Gade*, 1979; *Jenkins*, 1999]. We therefore represent submarine meltwater as fresh water with a virtual conservative temperature $\Theta_{mw}$,

$$\Theta_{mw} = \Theta_{sg} - \frac{L}{c_w} - \frac{c_i}{c_w}\left(\Theta_{sg} - \Theta_i\right), \tag{4}$$

which is equal to $\sim -90$°C where $\Theta_{sg}$ the temperature of the water at the phase transition temperature, $L$ is the latent heat of fusion (334 kJ kg$^{-1}$), $c_w$ the heat capacity of seawater (3947 J kg$^{-1}$ K$^{-1}$), $c_i$ the heat capacity of ice (2009 J kg$^{-1}$ K$^{-1}$), and $\Theta_i$ the ice temperature assumed to be $-15$°C [*Lüthi and Funk*, 2001]. This cold virtual temperature is due to the large amount of heat needed to melt ice.

By solving (2) for $f_e$ we can rewrite (1) and (3) as

$$f_{sg} + f_{mw} + \frac{S_A}{S_{A_e}} = 1, \tag{5}$$

and,

$$\Theta = \Theta_{sg} f_{sg} + \Theta_{mw} f_{mw} + \Theta_e \frac{S_A}{S_{A_e}}. \tag{6}$$

Finally, we can solve (5) for $f_{mw}$, and combine that with (6) for $f_{sg}$, which provides the two fractional water masses of interest,

$$f_{mw} = 1 - f_{sg} - \frac{S_A}{S_{A_e}}, \tag{7}$$

and

$$f_{sg} = \frac{1}{\Theta_{sg} - \Theta_{mw}} \left(\Theta - \Theta_{mw}\left[1 - \frac{S_A}{S_{A_e}}\right] - \Theta_e \frac{S_A}{S_{A_e}}\right). \tag{8}$$

### 3.2.2. Mixing Model Estimates

To estimate the different water mass fractions (subglacial discharge, submarine melt, and entrained water; equation (1)) using this method, we need to define the different water mass properties.

We assume that the subglacial discharge is freshwater that flows out at the grounding line ($z_{sg} = 150$ m) and therefore has conservative temperature, $\Theta_{sg}$, at the phase change temperature of $-0.13$°C ($<0$°C due to pressure $>1$ atm), and salinity, $S_{A_{sg}}$, of 0 g kg$^{-1}$.

The meltwater temperature, $\Theta_{mw}$, is defined in equation (4), and its salinity is assumed to be 0 g kg$^{-1}$.

We estimate the temperature and salinity of the entrained waters by averaging the mean temperature between 25 m and the bottom for all profiles collected within 100 m of the plume center. Properties of the entrained waters, the third end-member, derived using this approach are $S_{A_e} = 33.1$ g kg$^{-1}$ and $\Theta_e = 1.0$°C. The standard deviation of the vertically averaged temperatures within these profiles is 0.1°C.

Theoretical mixing lines for the three end-members are shown by the dashed lines in Figure 9. These lines are described by *Gade* [1979], *Jenkins et al.* [2010], and *Straneo et al.* [2011]. The mixing of subglacial discharge and entrained waters occurs on lines described by

$$\frac{d\Theta}{dS_A} = S_{A_e}^{-1}\left(\Theta_e - \Theta_{sg}\right). \tag{9}$$

The mixing of submarine melt and entrained water occurs on lines described by

$$\frac{d\Theta}{dS_A} = S_{A_e}^{-1}\left(\Theta_e - \Theta_i + \frac{c_i}{c_w}\left(\Theta_i - \Theta_{sg}\right) + \frac{L}{c_w}\right). \tag{10}$$

We note that the slopes of the subglacial discharge mixing lines in $\Theta - S_A$ space (equation (9), Figure 9) are $\sim$1°C per 30 $S_A$ units. This means that subglacial discharge changes the salinity of the ambient water by a factor of 30 more than it changes the temperature, and therefore freshness is indicative of subglacial discharge. The slopes of the submarine melt lines (equation (10), Figure 9) are $\sim$2.5°C per $S_A$ unit. This means that submarine melt changes the temperature by a factor of 2.5 more than the salinity, and therefore cooling is indicative of submarine melt.

### 3.3. Subglacial Discharge Fraction in the Pool

Given an entrained water salinity of $S_{A_e} = 33.1$ g kg$^{-1}$ and a plume pool salinity, $S_{A_p}$, between 29.8 and 32.4 g kg$^{-1}$, the subglacial discharge fraction $f_{sg}$ in the pool is 0.02–0.1 (equation (8), Figure 9). The mean subglacial discharge volume fraction in the JetYak pool surface samples is 0.07, and we use this value for the remainder of the paper. We note that the calculation of $f_{sg}$ for the pool waters is only weakly sensitive to the salinity of the entrained water properties because of the large difference between the fjord and pool properties.

### 3.4. Meltwater Fraction in the Pool

The bulk of the plume pool's properties lie on a line in $\Theta - S_A$ space that is parallel to, but slightly cooler than, the subglacial discharge line that marks 0% submarine meltwater fraction (Figure 9). This cooling ($\sim$0.1°C for the mean of the JetYak data) is attributed to ice melting according to the model described by (7) and (8), and the volumetric submarine meltwater fraction, $f_{mw}$, estimated by this method is 0.0006. We note, however, that this fraction is very sensitive to the choice of the entrained water temperature since it scales linearly with the temperature difference between the entrained waters, $\Theta_e$, and the observed water temperature (in this case that of the pool waters).

### 3.5. Subglacial Discharge Volumetric Flow Rate

By using the velocity measured by the JetYak's ADCP, we estimate the pool flux, $Q_p$, using the pool cross-sectional area, $A_p$, and mean velocity, $v_p$,

$$Q_p = v_p A_p. \tag{11}$$

We assume that the pool width at the surface is 200 m (from Figure 3). To estimate the cross-sectional area of the pool in the ice-parallel and vertical plane (the ($y$,$z$) plane, Figure 10), we calculate an upper bound by assuming it is a rectangle and a lower bound by assuming it is an inverted triangle, each with maximum depth $d_p$ of 20 m. Given this width and depth, the area of the pool in the $y$,$z$ plane against the ice falls in the range of 2000–4000 m$^2$. To estimate the mean along-plume velocity over this area, we use the extrapolated velocity profile shown in Figure 6. We assume it is representative of the plume center velocity orthogonal to the ice, and that the velocity decreases linearly to zero toward the edges of the pool. With the above assumptions, the volume flux within the pool, $Q_p$, is estimated to be between 1500 and 2000 m$^3$ s$^{-1}$, and we use $Q_p = 1750 \pm 250$ m$^3$ s$^{-1}$ as a mean value.

Given the estimated 0.07 volume fraction of subglacial discharge, $f_{sg}$, in the pool and the estimated volume flux, $Q_p$, we can estimate the subglacial discharge volume flux, $Q_{sg}$,

$$Q_{sg} = Q_p f_{sg}. \tag{12}$$

We obtain a volume flux of subglacial discharge in the pool from 105 to 140 m$^3$ s$^{-1}$. If we assume that the pool contains all of the subglacial discharge released at this location along the glacier front, then the

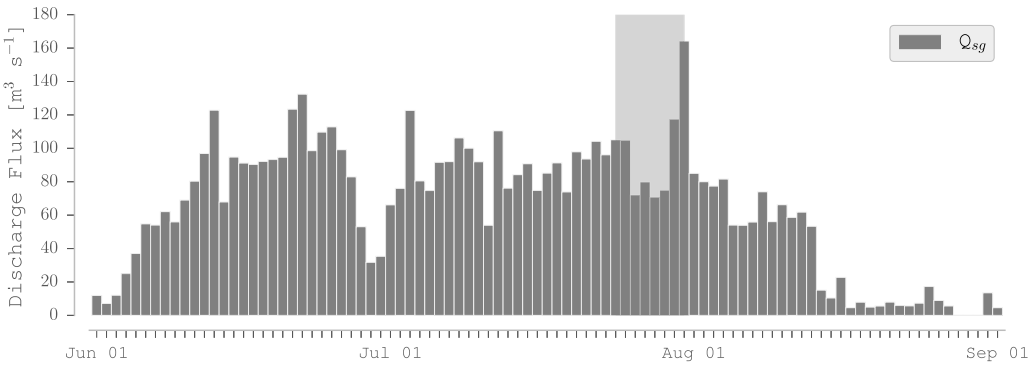


**Figure 11.** Subglacial discharge volume flux as calculated following the methods of *Stevens et al.* [2016] driven by daily RACMO runoff for 2013 [*van den Broeke et al*., 2009]. Discharge flux is only for the upstream glaciological catchment basin C1 defined in *Stevens et al*. [2016].

estimated subglacial discharge flux must be equal to the volume of subglacial discharge injected at the base of the glacier.

We compare this number with that estimated from the RACMO atmospheric model (RACMO model v2.3) [*van den Broeke et al*., 2009] for the upstream glaciological catchment basin defined in *Stevens et al*. [2016]. The drainage basin associated with the observed plume is the largest of the three catchment basins identified by *Stevens et al*. [2016] and is consistent with observations of a subsurface intrusion of glacially modified waters observed in 2012. Using RACMO estimated runoff for the 5 days prior to the velocity measurements on 26 July 2013, we calculate the daily average runoff from this catchment to be 101 $m^3\ s^{-1}$ (std 5.4 $m^3\ s^{-1}$; Figure 11). Our estimated subglacial discharge flux of 105 to 140 $m^3\ s^{-1}$ is ∼100%–140% of that estimated by RACMO.

In our analysis, we make the assumption that the fjord properties and subglacial discharge can be treated as approximately constant during the survey. This assumption is supported by estimates of subglacial discharge prior to and during our survey (Figure 11), and similarities in the surface signature of the plume during our survey and a month prior to it (Figures 1 and 3). Furthermore, CTD and XCTD data collected during our survey (Figure 5) suggest that the fjord properties are approximately constant during that period.

### 3.6. Submarine Meltwater Flux

We use the submarine meltwater fraction in the pool, $f_{mw}$, combined with the pool flux, $Q_p$, to estimate the submarine meltwater volumetric flow rate, $Q_m$,

$$Q_m = Q_p\, f_{mw}. \tag{13}$$

Given a submarine meltwater fraction of 0.0006 and a mean volume flux within the plume of 1750 $m^3\ s^{-1}$, the estimated submarine meltwater flux is ∼1 $m^3\ s^{-1}$, i.e., 2 orders of magnitude smaller than the subglacial discharge flux. The melt rate is addressed in section 5.

## 4. Models

Here we use an idealized plume model and a slightly more sophisticated model of a plume near an ice front to address two questions. First, do idealized plume models predict the plume characteristics inferred from our data? Second, to what extent do the submarine meltwaters or variations in the entrained water properties influence the behavior of the plume? Our first model is based on *Morton et al*. [1956], hereafter MTT, and we consider the self-similar solutions of this idealized plume model. The second model (J2011-M) is that of *Jenkins* [2011] but modified for a point source of subglacial discharge. The limitation of these models is that they can only represent the dynamics of the plume before it detaches from the ice face, consequently they cannot model the dynamics in the "pool" region and cannot be used to interpret the data far away from the ice face. Furthermore, the MTT self-similar solutions describe a plume that rises until it reaches the free surface due to the homogeneous ambient stratification. In the J2011-M model implementation used here, the integration stops when the plume density is greater than the ambient density. Hence, in this

study, neither the MTT self-similar solutions nor the J2011-M model can represent a plume "overshooting" its neutral density due to its vertical momentum.

### 4.1. MTT Self-Similar Solutions

We begin by using the point-source self-similar analytical solutions to the plume equations derived by *Morton et al.* [1956]. Self-similar solutions are valid in regions where the solutions do not depend on the details of the initial conditions or boundary conditions but where the system is still far from its final equilibrium state [*Barenblat*, 1996]. These solutions describe the plume radius, volume flux, and vertical velocity within the plume core below the plume pool and the density difference between the ambient waters and the plume core. They assume a homogeneous ambient fluid, that the plume has zero momentum and volume flux at the source (representing, for example, a plume generated by a heat source), and neglect the effect of added buoyancy flux due to submarine melt.

At each depth the plume radius, volume flux, vertical velocity, and the density difference between the ambient waters and the plume core are only a function of the subglacial discharge buoyancy flux for a given entrainment constant [*Morton et al.*, 1956]. The finite momentum and volume flux of the subglacial discharge are taken into account by using a "virtual origin" [*Hunt and Kaye*, 2001]. As discussed in *Cenedese and Linden* [2014], the virtual origin correction is the distance from the physical source that an imaginary pure plume has in order for the actual buoyancy, momentum and volume fluxes of the plume to be correct at the physical source. By imaginary plume, we mean a plume emanating from a point source at the virtual origin with zero momentum and volume fluxes but with the same buoyancy flux. We use this virtual origin correction because the equations introduced below are strictly valid for a pure plume, i.e., a plume for which buoyancy and momentum fluxes are balanced at the source [*Hunt and Kaye*, 2001]. Hence, the point-source self-similar solutions are initiated at a depth, $z_v$, below the physical source.

The virtual origin, $z_v$, is calculated using the expression of *Hunt and Kaye* [2001] knowing the volume flux, $Q_{sg}$, the buoyancy flux, $B_0 = Q_{sg}\, g'_0$ and the momentum flux, $M_0 = Q_{sg}^2/A$, at the source. In the above expressions, $A$ is the area of the source and $g'_0$ the reduced gravity calculated at the source ($z = 0$ m) which is defined in general as

$$g'(z) = \frac{g\,(\rho_a - \rho_p(z))}{\rho_0}, \tag{14}$$

where $g$ is gravity, $\rho_p(z)$ is the plume density, $\rho_a$ is the ambient density, and $\rho_0$ is a representative density, equal to the average of $\rho_a$ and $\rho_p$. We use the average value of the subglacial discharge estimate in section 3.5 ($Q_{sg} = 122.5$ m$^3$ s$^{-1}$), and a value of $g'_0 = 0.26$ m s$^{-2}$ obtained using the ambient temperature, $\Theta_e$, and salinity, $S_{A_e}$. For a radius of the source varying from 5 to 15 m, the value of the virtual origin ranges from 34 to 28 m, respectively. A volume flux of $Q_{sg} = 122.5$ m$^3$ s$^{-1}$ corresponds to a velocity at the source, considered to be a half-cylinder conduit, ranging from 3.1 to 0.3 m s$^{-1}$, for radii ranging from 5 to 15 m, respectively. There are no published observations of fluid velocities near the marine-terminating boundary of a subglacial conduit, but model studies have used velocities from $<$0.1 m s$^{-1}$ [*Salcedo-Castro et al.*, 2013], to 0.5 m s$^{-1}$ [*Salcedo-Castro et al.*, 2011; *Xu et al.*, 2013] up to 4 m s$^{-1}$ [*Xu et al.*, 2012]. Hence, the chosen range of values for the source radius, and consequently source velocity, are consistent with these modeling studies.

The MTT self-similar solutions produce a volume flux for a conical plume; because we are considering half of a conical plume (Figure 10), we apply a correction by doubling the initial values of $Q_{sg}$, hence doubling the source buoyancy flux $B_0$, and halving the resulting volume flux. Hence, the corrected expression for the volume flux of half-conical plume is, including the correction for the virtual origin, $z_v$:

$$Q = \left(\frac{1}{2}\right)\left(\frac{6}{5}\right)\left(\frac{9}{10}\right)^{\frac{1}{3}} \pi^{\frac{2}{3}}\, \alpha^{\frac{4}{3}}\, (2\,B)^{\frac{1}{3}}\, (z + z_v)^{\frac{5}{3}}, \tag{15}$$

where $\alpha$ is the entrainment constant equal to 0.1, $z$ the height of the plume above the source, and $B = g'Q = B_0$ is the buoyancy flux which is conserved in a plume. The value of the entrainment parameter $\alpha$ is within the range used for geophysical processes [*Carazzo et al.*, 2008] and typical of glacial fjord studies [see *Straneo and Cenedese*, 2015].

Furthermore, we can calculate vertical velocity, $w$, reduce gravity, $g'$, and radius, $r$, of the plume as a function of depth using the MTT solutions with the correction for the half-conical plume:

$$w = \frac{5}{6\alpha}\left(\frac{9}{10}\alpha(2B)\right)^{\frac{1}{3}}\pi^{-\frac{1}{3}}(z+z_v)^{-\frac{1}{3}}, \tag{16}$$

$$g' = \frac{5B}{6\alpha}\left(\frac{9}{10}\alpha(2B)\right)^{-\frac{1}{3}}\pi^{-\frac{2}{3}}(z+z_v)^{-\frac{5}{3}}, \tag{17}$$

$$r = \frac{6}{5}\alpha(z+z_v). \tag{18}$$

We neglect any changes introduced by the ice boundary other than the fact that it reduces the plume in half. This is equivalent to assuming that the ice boundary is frictionless, as assumed in some plume modeling studies [for example, *Kimura et al.*, 2014; *Slater et al.*, 2015]. Finally, this model does not take into account the contribution of melt water to the plume. This approach has been applied successfully before in a similar setting [*Cenedese and Gatto*, 2016].

### 4.2. J2011-M Model

The MTT self-similar solutions described above provide an estimate of volume flux, velocity, density difference, and radius. However, they lack many processes that occur when a subglacial discharge plume rises along and melts a glacier face. In particular, nonhomogeneous stratification of the fjord waters, drag from the ice face, and the impact of submarine melt on the plume buoyancy flux are not included in the idealized MTT model.

The *Jenkins* [2011] model evolved from the same conservation equations used to obtain the MTT self-similar solutions, permitting a more complex environment but relying on the same core plume physics. It uses a stream tube approach to model the plume and includes a thermodynamical submarine melt rate parameterization of the ice-ocean boundary based on the three equations model of *Hellmer and Olbers* [1989] and *Holland and Jenkins* [1999]. Hence, this model provides an estimate of melting and accounts for the change in buoyancy flux within the plume core due to the addition of submarine meltwater. It is 1-D, steady state, and reports results as a function of distance from the source. It solves four conservative equations for mass, momentum, heat, and salt [*Jenkins*, 2011] and is used as a common comparison in the subglacial discharge plume modeling literature [see for example, *Sciascia et al.*, 2013; *Kimura et al.*, 2014; *Cowton et al.*, 2015]. The submarine melting included in this model is derived from a parameterization [*Holland and Jenkins*, 1999] which, in turn, depends on coefficients that are not well constrained [*Straneo and Cenedese*, 2015]. We use a version of the model (hereafter J2011-M) that is modified for a point source of subglacial discharge [*Kimura et al.*, 2014; *Cowton et al.*, 2015; *Stevens et al.*, 2016] rather than a line source as in *Jenkins* [2011].

This model can also support stratification of the ambient entrained waters, and we use both constant values for the ambient temperature, $\Theta_e$, and salinity, $S_{A_e}$, and the mean (maintaining the vertical dimension) of all profiles within 100 m of the center of the plume/ice edge (a subset of the bold lines in Figure 5). We run it with a vertical ice wall at $-15$°C [*Lüthi and Funk*, 2001]. The results are not sensitive to the ice temperature because most heat is transferred during the phase change, not warming the subzero ice to the melting point. We use values of the thermal and diffusion Stanton numbers equal to $C_D^{1/2}\Gamma_T = 0.0011$ and $C_D^{1/2}\Gamma_S = 3.1 \times 10^{-5}$, respectively [*Jenkins et al.*, 2010; *Jenkins*, 2011; *Sciascia et al.*, 2013], and the same fixed $\alpha$ entrainment constant equal to 0.1 used in the MTT self-similar solutions. The model is forced with an initial volume flux of $Q_{sg} = 122.5$ m$^3$ s$^{-1}$ and reduced gravity $g'_0 = 0.26$ m s$^{-2}$ as in the MTT self-similar solutions. The initial plume's velocity and radius in the J2011-M model are obtained from balancing the buoyancy and frictional terms at the source in the momentum equation. Since self-similar solutions are valid in regions where the solutions do not depend on the details of the initial conditions or boundary conditions [*Barenblat*, 1996], we expect the J2011-M model solutions to asymptotically approach the self-similar solutions only away from the source and for a distance approaching infinity. Indeed, Figure 12 illustrates that the two solutions are converging for increasing values of the distance from the source.

### 4.3. Model Results

The results from the two plume models described above are presented in what follows from the least to the more complex scenario.

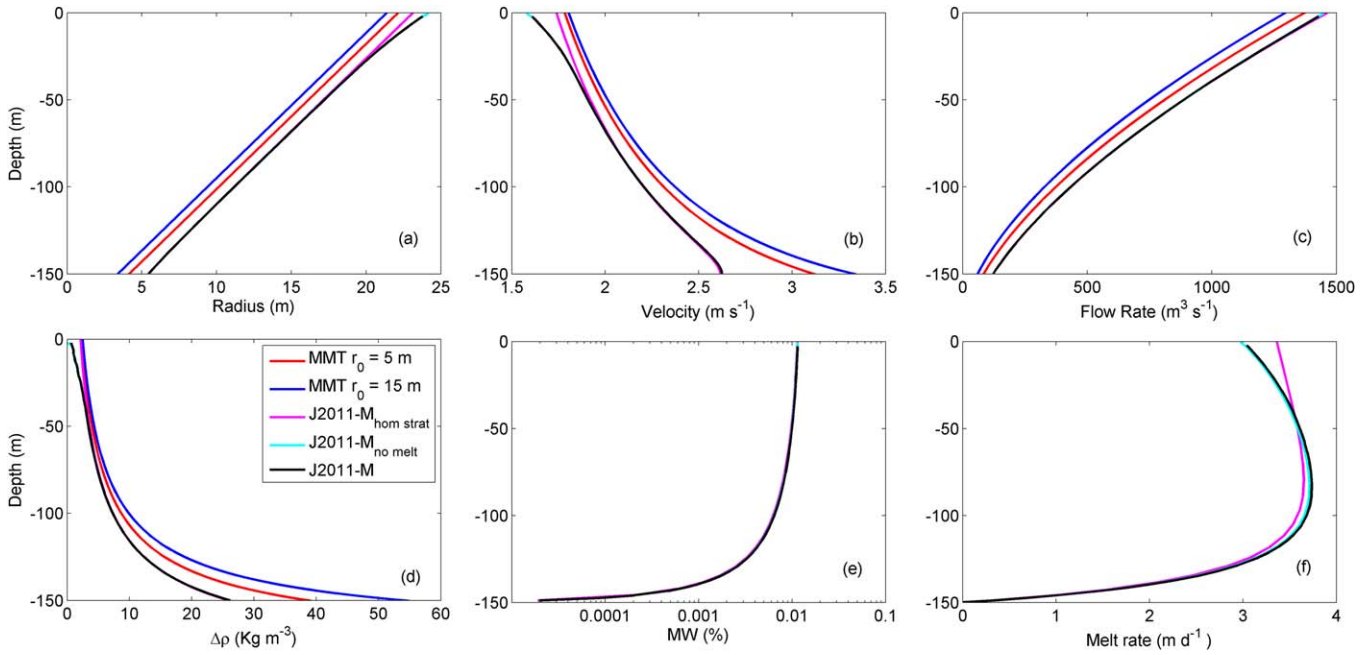


**Figure 12.** MTT self-similar solutions (blue and red lines) and J2011-M model (black, cyan, and magenta lines) for the (a) plume radius, (b) vertical velocity, (c) volume flux, (d) density difference between the plume and ambient waters, (e) melt water fraction, and (f) melt rate. MTT self-similar solutions were obtained for two different values of the source radius, r = 5 m (red lines) and r = 15 m (blue lines) and homogeneous ambient stratification. Magenta and cyan lines are not VISIBLE or are barely visible because they are almost identical to the black lines which overlay them.

*MTT self-similar solutions*. The simplest model is the idealized MTT model which has analytical self-similar solutions for the plume variables. Equation (15) gives an estimate of the volume flux at the free surface, i.e., 150 m above the physical source, equal to 1374 $m^3\ s^{-1}$ for a source radius of 5 m, and 1296 $m^3\ s^{-1}$ if the source radius is 15 m. Compared to our pool volume flux estimate of 1750 $\pm$ 250 $m^3\ s^{-1}$ the self-similar solutions under predicts the estimated pool volume flux. Plume vertical velocity and radius at the surface for a source radius of 5 m are 1.8 m $s^{-1}$ and 22 m, respectively, and 1.8 m $s^{-1}$ and 21 m for a 15 m radius source. The self-similar solutions for plume vertical velocity, flow rate, radius, and density difference between the plume and ambient waters at all depths are shown in Figure 12, where the red and blue solid lines represent a source radius of 5 and 15 m, respectively. It is worth noting that a source radius of 5 m produces a "forced" plume, i.e., at the source the momentum flux is larger than the buoyancy flux, while a source radius of 15 m generates a "lazy" plume, i.e., at the source the buoyancy flux is larger than the momentum flux [*Hunt and Kaye*, 2001]. The radius of the lazy plume (i.e., source radius of 15 m) near the source (i.e., $z = -150$ m) is much smaller than the source radius because a plume having a much larger buoyancy flux than momentum flux contracts reducing its radius and increasing its velocity [*Hunt and Kaye*, 2001].

*J2011-M model with homogeneous stratification and melt/drag*. The first run with the J2011-M model is with the same homogeneous ambient waters as the MTT self-similar solutions but with a changing buoyancy flux in the plume due to meltwater and the drag induced by the ice face (Figure 12, magenta lines). Far away from the source the results are approaching those obtained with the MTT self-similar solutions suggesting that the influence of drag and buoyancy flux due to meltwater are both minimal for this plume.

*J2011-M model with observed stratification and drag but no melt*. In the second run, we consider the observed stratification but neglect the impact on the plume of the additional buoyancy flux due to the submarine meltwater, hence conserving the buoyancy flux in the plume (cyan lines Figure 12). As expected, the results are very similar to those obtained in the first run and, far away from the source, they approach the MTT self-similar solutions. However, the submarine melt rate (Figure 12f) in the top 50 m is reduced due to the slightly cooler waters in this region (Figure 5) and the slightly smaller vertical velocity in the plume, the latter a consequence of the reduced difference in density between the plume and ambient waters (Figure 12b).

*J2011-M model with observed stratification and melt/drag*. The third more realistic run is similar to the second but now we allow the buoyancy flux in the plume to change as a result of the addition of submarine meltwater (black lines in Figure 12).

The solutions of the second and third runs are almost identical as indicated by the almost perfect overlap of the black solid lines over the cyan lines in Figure 12. This result suggests that the plume is in a "convection-driven" melting regime in which the subglacial discharge is the main buoyancy source of the plume with only a small contribution from submarine melting [*Motyka et al*., 2003; *Jenkins*, 2011].

In the more realistic J2011-M model run (Figure 12, black lines), the volume flux near the surface is $\sim$1430 $m^3\ s^{-1}$ (Figure 12c) a value similar to that obtained with the MTT self-similar solutions and slightly closer to the estimated volume flux in the pool ($Q_p = 1750 \pm 250\ m^3\ s^{-1}$). The under prediction of the estimated pool volume flux by both models is perhaps due to further entrainment occurring as the plume evolves into the pool. The plume's temperature and salinity near the surface are 0.89°C and 30 g $kg^{-1}$ which are in excellent agreement with the observed temperature (0.8–1°C) and salinity (30–32 g $kg^{-1}$) measured in the pool (Figure 9). The value of the plume radius and vertical velocity near the surface are 24 m and 1.6 m $s^{-1}$ (Figures 12a and 12b), respectively, similar to the results from the more idealized MTT self-similar solutions.

## 5. Submarine Melt Rates

Given the observation-based estimate of submarine meltwater volume flux of 1 $m^3\ s^{-1}$, and assuming one knows the area over which this melting occurred, one can in principle estimate the melt rate per unit area ("melt rate" hereafter). We stress that this calculation is highly uncertain both because of the already mentioned uncertainties in the meltwater fraction estimate and, also, because we have no way of knowing over which area the submarine melting occurred (including whether it occurred in the plume). Nonetheless it is useful to discuss several scenarios.

If one assumes that all of the 1 $m^3\ s^{-1}$ originated from submarine melting within the plume—and assuming a plume area equivalent to a triangle of width $\sim$40 m (the diameter of the plume at the surface, from model results) and height $\sim$150 m (yielding an area of 3000 $m^2$)—this implies a melt rate in the plume of $\sim$50 m $d^{-1}$! This is unrealistically high, and inconsistent with the slow ice velocity and our visual observations of the glacier's relatively stable ice frontal positions over the survey period. Even by expanding the area to include that of the pool in contact with the glacier face ($\sim 200 \times 20\ m = 4000\ m^2$)—the melt rate will only reduce by a factor of 2—still yielding what seems like an unreasonable estimate.

It seems more likely instead that the submarine meltwater volume flux has been overestimated, due to uncertainties in the meltwater fraction prediction, and/or that the meltwater flux is due to melting that occurred elsewhere. Support for the latter is provided by the presence of a cold layer along the glacier front outside the plume region (Figure 8 (X1)). The fact that these waters are found all along the glacier, and that they are coldest away from the plume region, suggests that they are formed as a result of submarine melting along a wider swath of the glacier face than just within the plume. Indeed, their distribution in $\Theta - S_A$ space is largely along melt lines (Figure 9). We speculate that if this submarine meltwater is entrained in the plume and discharged at the surface in the pool, it would skew the estimates of submarine melt rates occurring in the plume region.

Using the MTT self-similar solutions, we can calculate the volume flux of entrained water as a function of depth which can be combined with the submarine meltwater fraction profiles, within 100 m of the center of the plume/ice edge, to obtain a vertical profile of volume flux of meltwater into the plume due to entrainment. The integral of this profile provides an estimate of the meltwater fraction in the plume at the surface due solely to entrainment of meltwater. This value is 0.0008 and comparable to the estimated value of 0.0006 obtained using the data in Figure 9. This result suggests that the meltwater fraction measured in the plume pool is composed mainly of meltwater entrained in the plume and only a very small fraction of it is from the actual melting of the glacier face covered by the plume.

This result is supported by the melt rate estimates from the J2011-M model shown in Figure 12. The volume flux of meltwater at the surface is $\sim$0.14 $m^3\ s^{-1}$, an order of magnitude smaller than the 1 $m^3\ s^{-1}$ meltwater flux estimated from our data and, not surprisingly, comparable to values estimated by models using similar parameterizations [e.g., *Kimura et al*., 2014; *Slater et al*., 2015].

## 6. Discussion

We have provided several key findings relating to a localized plume forced by subglacial discharge at the edge of Saqqarliup Sermia, a midsized Greenlandic outlet glacier. We have confirmed that the localized sediment-laden patches of water observed at the surface of Saqqarliup Fjord near the ice edge (and observed near the margin of many Greenland glaciers) contain modified deep waters which have upwelled as a result of the injection of fresh water at depth (i.e., subglacial discharge). In this case, these surface waters were associated with a horizontal jet spreading away from the glacier with velocities up to 3 m $s^{-1}$. This feature rapidly disappears below the surface a few hundreds of meters from the glacier face, suggesting that the modified deep waters overshot their neutral density level. Their volume flux was on the order of $1750 \pm 250$ $m^3$ $s^{-1}$.

From property analysis, we estimated the subglacial discharge fraction to be up to 10% in the surface expression of the plume (i.e., the entrainment of ambient water in the plume core diluted the initial discharge by a ratio of 10:1 or more). The implication is that the volume flux associated with the plume increased by an order of magnitude from its origin to the surface. The data also confirm that plumes can overshoot their neutral density and showed that a continuously forced plume can maintain a large horizontal density gradient with the surrounding ambient water.

Using the estimated subglacial discharge rate (section 3.5), we have shown that the observed volume flux in the pool region is consistent with that predicted by an idealized half-conical plume model (MTT) forced by a localized discharge. This provides the first evidence that plume theory can adequately reproduce the broad features of plumes at the edge of a glacier. Using plume theory, furthermore, we have estimated the radius of the plume to be about 20 m and the vertical velocities to be on the order of 1.8 m $s^{-1}$ near the surface. The implication is that these plumes are very narrow localized features whose pool surface expressions may be an order of magnitude larger than the feature itself.

Estimates of the submarine meltwater flux associated with the observed plume are uncertain due to the sensitivity of the meltwater fraction estimate to the entrained water properties. Our estimated submarine meltwater fraction of 0.0006 means the volume flux of submarine meltwater is 3 orders of magnitude smaller than that of the entrained ambient water, and 2 orders of magnitude smaller than that of the subglacial discharge. These values are consistent with the plume models predictions and with the fractions of submarine meltwater and subglacial discharge computed using noble gases in Atâ Sund, within a few kilometers of the terminus of a similar midsized glacier in West Greenland [*Beaird et al*., 2015]—especially if one assumes that further dilution of both glacial meltwater sources has occurred with increasing distance from the glacier.

If we assume the estimated submarine meltwater flux is due to melting over the plume area only, it gives rise to melt rates of 25–50 m $d^{-1}$, which seem unrealistically large. One plausible explanation for this is that the inferred submarine meltwater flux contains meltwater that originated elsewhere along the glacier front which is then entrained into the plume. This inference is supported by the fact that the coldest waters are found all along the glacier face and not just in the plume region. It is also consistent with melt rates derived from idealized plume models, coupled with a melt rate parameterization, which are lower than the data based estimate. This could be coincidental, however, because the coefficients used in these melt rate parameterizations are largely untested.

## 7. Conclusions

We have presented measurements collected within 100 m of the ice front in and through the surface expression of a subglacial discharge plume, here termed the plume pool. We have used these data to describe the plume size and characteristics, including plume volume flux, subglacial discharge volume flux, subglacial discharge fraction in the plume, meltwater fraction in the plume, and melt rate.

The plume overshoots its neutral density level due to its high vertical velocity and is visible at the fjord surface as an anomalously cold and salty pool. At the surface it flows away from the ice with high horizontal velocity (up to 3 m $s^{-1}$). Approximately 300 m from the glacier face, the plume waters are no longer visible at the surface as they descend to reach their neutrally buoyant level. The subglacial discharge fraction in the plume pool waters is $\sim$10%, the submarine meltwater fraction is $<$0.1%, and the remaining $\sim$90% are

entrained fjord waters. The observed flux of subglacial discharge at the fjord surface matches the expected subglacial discharge obtained from an atmospheric-driven Greenlandic ice sheet runoff-model combined with a subglacial catchment routing model. At the surface, the volume flux of the plume is $\sim 1750 \pm 250$ m$^3$ s$^{-1}$, in agreement with the prediction obtained from plume theory. From this theory the radius and vertical velocity below the pool are $\sim$20 m and $\sim$1.8 m s$^{-1}$, respectively, indicating that the surface expression of the plume pool observed in Figures 1 and 3 covers a much larger area than the top of the plume core. Furthermore, not only does the surface volume flux of the modeled plume match the observations reasonably well, but the modeled plume temperature and salinity at the surface also match those observed in the field. The inclusion of submarine melt in the plume buoyancy flux and the drag exerted from the ice face appear to have a negligible impact on the plume dynamics. In this particular setting, at Saqqarliup Sermia, the effects due to a nonhomogeneous stratification are small and the very simple analytical MTT self-similar solutions can be used to predict the plume variables. However, it should be noted that in fjords in which a strong stratification is present the validity of the MTT self-similar solutions assumption of uniform stratification is no longer valid and a more complex model such as the J2011-M may be needed.

Melt rates derived assuming that all of the meltwater flux is due to melting occurring at the plume/glacier interface are unreasonably high. This could be due to errors in estimating the meltwater fraction or to the entrainment of meltwater that was formed elsewhere along the glacier front. This latter hypothesis is supported by the existence of a band of cold water along the glacier front, at a depth of about 20 m, outside the plume region.

**Acknowledgments**

Data are available from F. Straneo (fstraneo@whoi.edu). Support was provided by the National Science Foundation (NSF) through PLR-1418256 to F.S., S.B.D., and H.S.; OCE-1434041 to F.S. and C.C.; and through the Woods Hole Oceanographic Institution (WHOI) Ocean and Climate Change Institute (OCCI) Arctic Research Initiative to F.S., S.B.D., and H.S. K.D.M. was supported by a OCCI post-graduate fellowship through the WHOI Postdoctoral Scholar Program, and during the field campaign by National Aeronautics and Space Administration's (NASA) Headquarters under the NASA Earth and Space Science Fellowship Program (grant NNX10AN83H). The authors would like to acknowledge J. Pietro, L. Stevens, and Ove Villadsen for help and support during the fieldwork; M. R. van den Broeke for RACMO data, and L. Stevens for 2013 subglacial discharge estimates. We thank C. Gladish and the anonymous reviewers for their comments.

## References

Bamber, J. L., M. R. van den Broeke, J. Ettema, J. Lenaerts, and E. J. Rignot (2012), Recent large increases in freshwater fluxes from Greenland into the North Atlantic, *Geophys. Res. Lett.*, *39*, L19501, doi:10.1029/2012GL052552.

Barenblat, G. I. (1996), *Scaling, Self-Similarity, and Intermediate Asymptotics: Dimensional Analysis and Intermediate Asymptotics*, Cambridge Univ. Press, Cambridge, U. K.

Beaird, N., F. Straneo, and W. Jenkins (2015), Spreading of Greenland meltwaters in the ocean revealed by noble gases, *Geophys. Res. Lett.*, *42*, 7705–7713, doi:10.1002/2015GL065003.

Bendtsen, J., J. Mortensen, K. Lennert, and S. Rysgaard (2015), Heat sources for glacial ice melt in a West Greenland tidewater outlet glacier fjord: The role of subglacial freshwater discharge, *Geophys. Res. Lett.*, *42*, 4089–4095, doi:10.1002/2015GL063846.

Bjørk, A. A., L. M. Kruse, and P. B. Michaelsen (2015), Brief communication: Getting Greenland's glaciers right—A new dataset of all official Greenlandic glacier names, *Cryosphere*, *9*(6), 2215–2218, doi:10.5194/tc-9-2215-2015.

Carazzo, G., E. Kaminski, and S. Tait (2008), On the rise of turbulent plumes: Quantitative effects of variable entrainment for submarine hydrothermal vents, terrestrial and extra terrestrial explosive volcanism, *J. Geophys. Res.*, *113*, B09201, doi:10.1029/2007JB005458.

Carroll, D., D. A. Sutherland, E. L. Shroyer, J. D. Nash, G. A. Catania, and L. A. Stearns (2015), Modeling turbulent subglacial meltwater plumes: Implications for fjord-scale buoyancy-driven circulation, *J. Phys. Oceanogr.*, *45*(8), 2169–2185, doi:10.1175/JPO-D-15-0033.1.

Cenedese, C., and V. M. Gatto (2016), Impact of two plumes' interaction on submarine melting of tidewater glaciers: A laboratory study, *J. Phys. Oceanogr.*, *46*(1), 361–367, doi:10.1175/JPO-D-15-0171.1.

Cenedese, C., and P. F. Linden (2014), Entrainment in two coalescing axisymmetric turbulent plumes, *J. Fluid Mech.*, *752*, doi:10.1017/jfm.2014.389.

Chauché, N., A. Hubbard, J.-C. Gascard, J. E. Box, R. Bates, M. Koppes, A. Sole, P. Christoffersen, and H. Patton (2014), Ice–ocean interaction and calving front morphology at two west Greenland tidewater outlet glaciers, *Cryosphere*, *8*, 1457–1468, doi:10.5194/tc-8-1457-2014.

Chu, V. W. (2013), Greenland ice sheet hydrology: A review, *Prog. Phys. Geogr.*, *1*, 1–36, doi:10.1177/0309133313507075.

Cowton, T. R., D. Slater, A. Sole, D. Goldberg, and P. Nienow (2015), Modeling the impact of glacial runoff on fjord circulation and submarine melt rate using a new subgrid-scale parameterization for glacial plumes, *J. Geophys. Res. Oceans*, *120*, 796–812, doi:10.1002/2014JC010324.

Enderlin, E. M., and I. M. Howat (2013), Submarine melt rate estimates for floating termini of Greenland outlet glaciers (2000–2010), *J. Glaciol.*, *59*(213), 67–75, doi:10.3189/2013JoG12J049.

Enderlin, E. M., I. M. Howat, S. Jeong, M.-J. Noh, J. H. van Angelen, and M. R. van den Broeke (2014), An improved mass budget for the Greenland ice sheet, *Geophys. Res. Lett.*, *41*, 866–872, doi:10.1002/2013GL059010.

Gade, H. G. (1979), Melting of ice in sea water: A primitive model with application to the Antarctic ice shelf and icebergs, *J. Phys. Oceanogr.*, *9*, 189–198, doi:10.1175/1520-0485(1979)009<0189:MOIISW>2.0.CO;2.

Hartley, C. H., and M. J. Dunbar (1938), On the hydrographic mechanism of the so-called brown zones associated with tidal glaciers, *J. Mar. Res.*, *1*(4), 305–311.

Hellmer, H. H., and D. J. Olbers (1989), A two-dimensional model for the thermohaline circulation under an ice shelf, *Antarct. Sci.*, *1*(4), 325–336.

Holland, D. M., and A. Jenkins (1999), Modeling thermodynamic ice-ocean interactions at the base of an ice shelf, *J. Phys. Oceanogr.*, *29*(8), 1787–1800, doi:10.1175/1520-0485(1999)029<1787:MTIOIA>2.0.CO;2.

Hunt, G. R., and N. B. Kaye (2001), Virtual origin correction for lazy turbulent plumes, *J. Fluid Mech.*, *435*, 377–396, doi:10.1017/S0022112001003871.

Jenkins, A. (1999), The impact of melting ice on ocean waters, *J. Phys. Oceanogr.*, *29*, 2370–2381, doi:10.1175/1520-0485(1999)029<2370:TIOMIO>2.0.CO;2.

Jenkins, A. (2011), Convection-driven melting near the grounding lines of ice shelves and tidewater glaciers, *J. Phys. Oceanogr.*, *41*(12), 2279–2294, doi:10.1175/JPO-D-11-03.1.

Jenkins, A., P. Dutrieux, S. S. Jacobs, S. D. McPhail, J. R. Perrett, A. T. Webb, and D. White (2010), Observations beneath Pine Island Glacier in West Antarctica and implications for its retreat, *Nat. Geosci.*, *3*(7), 468–472, doi:10.1038/ngeo890.

Joughin, I. R., S. B. Das, G. E. Flowers, M. D. Behn, R. B. Alley, M. A. King, B. E. Smith, J. L. Bamber, M. R. van den Broeke, and J. H. van Angelen (2013), Influence of ice-sheet geometry and supraglacial lakes on seasonal ice-flow variability, *Cryosphere*, *7*(4), 1185–1192, doi:10.5194/tc-7-1185-2013.

Kimball, P., et al. (2014), The WHOI Jetyak: An autonomous surface vehicle for oceanographic research in shallow or dangerous waters, in *2014 IEEE/OES Autonomous Underwater Vehicles (AUV)*, pp. 1–7, Inst. of Electr. and Electr. Eng., Oxford, Miss., doi:10.1109/AUV.2014.7054430.

Kimura, S., P. R. Holland, and A. Jenkins (2014), The effect of meltwater plumes on the melting of a vertical glacier face, *J. Phys. Oceanogr.*, *44*, 3099–3117, doi:10.1175/JPO-D-13-0219.1.

Kjeldsen, K. K., J. Mortensen, J. Bendtsen, D. Petersen, K. Lennert, and S. Rysgaard (2014), Ice-dammed lake drainage cools and raises surface salinities in a tidewater outlet glacier fjord, West Greenland, *J. Geophys. Res. Earth Surf.*, *119*(6), 1310–1321, doi:10.1002/2013JF003034.

Lüthi, M. P., and M. Funk (2001), Modelling heat flow in a cold, high-altitude glacier: Interpretation of measurements from Colle Gnifetti, Swiss Alps, *J. Glaciol.*, *47*(157), 314–324, doi:10.3189/172756501781832223.

McDougall, T. J., and P. M. Barker (2011), *Getting Started with TEOS-10 and the Gibbs Seawater (GSW) Oceanographic Toolbox*, v 3.05, 28 pp., May 2015, SCOR/IAPSO WG127.

Mortensen, J., J. Bendtsen, R. J. Motyka, K. Lennert, M. Truffer, M. Fahnestock, and S. Rysgaard (2013), On the seasonal freshwater stratification in the proximity of fast-flowing tidewater outlet glaciers in a sub-Arctic sill fjord, *J. Geophys. Res. Oceans*, *118*, 1382–1395, doi:10.1002/jgrc.20134.

Morton, B. R., G. Taylor, and J. S. Turner (1956), Turbulent gravitational convection from maintained and instantaneous sources, *Proc. R. Soc. London, Ser. A*, *234*, 1–23, doi:10.1098/rspa.1956.0011.

Motyka, R. J., L. Hunter, K. A. Echelmeyer, and C. Connor (2003), Submarine melting at the terminus of a temperate tidewater glacier, LeConte Glacier, Alaska, U.S.A., *Ann. Glaciol.*, *36*(1), 57–65.

Motyka, R. J., W. P. Dryer, J. M. Amundson, M. Truffer, and M. Fahnestock (2013), Rapid Submarine Melting Driven by Subglacial Discharge, LeConte Glacier, Alaska, *Geophys. Res. Lett.*, *40*, 5153–5158, doi:10.1002/grl.51011.

O'Leary, M., and P. Christoffersen (2013), Calving on tidewater glaciers amplified by submarine frontal melting, *Cryosphere*, *7*, 119–128, doi:10.5194/tc-7-119-2013.

Salcedo-Castro, J., D. Bourgault, and B. deYoung (2011), Circulation induced by subglacial discharge in glacial fjords: Results from idealized numerical simulations, *Cont. Shelf Res.*, *31*(13), 1396–1405, doi:10.1016/j.csr.2011.06.002.

Salcedo-Castro, J., D. Bourgault, S. J. Bently, and B. deYoung (2013), Non-hydrostatic modeling of cohesive sediment transport associated with a subglacial buoyant jet in glacial fjords: A process-oriented approach, *Ocean Modell.*, *63*, 30–39, doi:10.1016/j.ocemod.2012.12.005.

Sciascia, R., F. Straneo, C. Cenedese, and P. Heimbach (2013), Seasonal variability of submarine melt rate and circulation in an East Greenland fjord, *J. Geophys. Res. Oceans*, *118*(5), 2492–2506, doi:10.1002/jgrc.20142.

Slater, D. A., P. W. Nienow, T. R. Cowton, D. N. Goldberg, and A. J. Sole (2015), Effect of near-terminus subglacial hydrology on tidewater glacier submarine melt rates, *Geophys. Res. Lett.*, *42*, 2861–2868, doi:10.1002/2014GL062494.

Stevens, L. A., F. Straneo, S. B. Das, A. J. Plueddemann, A. L. Kukulya, and M. Morlighem (2016), Linking glacially modified waters to catchment-scale subglacial discharge using autonomous underwater vehicle observations, *Cryosphere*, *10*, 417–432, doi:10.5194/tc-10-417-2016.

Straneo, F., and C. Cenedese (2015), The dynamics of Greenland's glacial fjords and their role in climate, *Annu. Rev. Mar. Sci.*, *7*(1), 89–112, doi:10.1146/annurev-marine-010213-135133.

Straneo, F., R. G. Curry, D. A. Sutherland, G. S. Hamilton, C. Cenedese, K. Vge, and L. A. Stearns (2011), Impact of fjord dynamics and glacial runoff on the circulation near Helheim Glacier, *Nat. Geosci.*, *4*(5), 322–327, doi:10.1038/ngeo1109.

Straneo, F., D. A. Sutherland, D. M. Holland, C. Gladish, G. S. Hamilton, H. L. Johnson, E. J. Rignot, Y. Xu, and M. Koppes (2012), Characteristics of ocean waters reaching Greenlands glaciers, *Ann. Glaciol.*, *53*(60), 202–210, doi:10.3189/2012AoG60A059.

van den Broeke, M. R., J. L. Bamber, J. Ettema, E. J. Rignot, E. Schrama, W. J. van de Berg, E. van Meijgaard, I. Velicogna, and B. Wouters (2009), Partitioning recent Greenland mass loss, *Science*, *326*(5955), 984–986, doi:10.1126/science.1178176.

Xu, Y., E. J. Rignot, D. Menemenlis, and M. Koppes (2012), Numerical experiments on subaqueous melting of Greenland tidewater glaciers in response to ocean warming and enhanced subglacial runoff, *Ann. Glaciol.*, *53*(60), 229–234, doi:10.3189/2012AoG60A139.

Xu, Y., E. J. Rignot, I. Fenty, and D. Menemenlis (2013), Subaqueous melting of Store Glacier, West Greenland from three-dimensional, high-resolution numerical modeling and ocean observations, *Geophys. Res. Lett.*, *40*, 4648–4653, doi:10.1002/grl.50825.